

# Characterization of Annealing Effects in Ultra-Shallow Boron-Implanted Si Wafers using Raman Scattering

Masashi Fukumoto<sup>a</sup>, Hiroaki Minami<sup>a</sup>, Noriyuki Hasuike<sup>a</sup>, Hiroshi Harima<sup>a</sup>, Masahiro Yoshimoto<sup>a</sup> and Woo Sik Yoo<sup>b</sup>

<sup>a</sup>Kyoto Institute of Technology, Matsugasaki, Sakyo, Kyoto 606-8585, Japan

<sup>b</sup>WaferMasters, Inc., San Jose, CA 95112, USA

Raman scattering was used as a non-contact and non-destructive characterization technique to present a systematic study on the crystallinity and diffusion of impurities in ultra-shallow ion-implanted Si wafers. In this study, the samples were prepared by the implantation of Si (100) wafers with B. The thermal annealing was carried out to investigate the effect of annealing under various conditions. The crystallinity of the samples was deteriorated with increase in B implantation level. Especially, near the surface, the crystallinity was seriously deteriorated, and the Raman spectra showed the generation of the amorphous Si phase. By thermal annealing, the surface amorphous Si was re-crystallized, and the implanted B was diffused enough to the top surface region. Furthermore, by using an N<sub>2</sub> and O<sub>2</sub> gas mixture, as an annealing atmosphere, promoted the recrystallization of surface amorphous Si and improved suppression of diffusion of the implanted B.

## Introduction

Formation of ultra shallow junctions is a key issue for development of miniaturization technologies in LSI [1]. For this purpose, ultra shallow ion implantation is required, as well as a novel annealing technique to activate the dopants and to recover the crystal quality of the implanted region without significant diffusion of the dopant species. Needless to say, such technology cannot be developed without precise characterization of impurity concentration profiles and junction depths. Usually, the effects of annealing are characterized in terms of sheet resistance measured by a four-point probe along with depth profiles of dopants [2,3]. However, a quick and non-destructive characterization technique is necessary for in-line process monitoring in semiconductor manufacturing environments.

In this work we focused on Raman scattering, which is a non-contact and non-destructive characterization technique requiring no special sample preparation. Despite its simplicity, Raman scattering provides useful information on materials. For example, one can easily evaluate the residual stress and crystallinity (long-range lattice ordering) with depth by using probe lasers with different penetration depths (wavelengths)[4,5]. Especially, Raman spectroscopy using UV lasers for excitation is an ideal tool for characterizing surface regions because the laser penetration depth is typically less than 10 nm in Si [1].

In this study, Si wafers with shallow implantation of B were characterized by Raman scattering using UV and visible lasers for excitation. Variation of crystallinity and impurity diffusion with depth were analyzed by selecting the appropriate laser

wavelength for excitation. The annealing effects were investigated by changing the annealing temperature and environment.

## Experiment

We prepared two types of Si (100) wafer samples, which were ion-implanted with  $^{11}\text{B}$  at an acceleration voltage of 5 kV and doses of  $2 \times 10^{14} \text{ cm}^{-2}$  and  $2 \times 10^{15} \text{ cm}^{-2}$ . A simulation shows that the boron density peaks at the depth of  $\sim 20 \text{ nm}$  for this acceleration voltage [6]. The samples were annealed at  $1005\text{--}1045^\circ\text{C}$  for 10 – 45 sec in an environment of pure  $\text{N}_2$  gas or  $\text{N}_2$  and  $\text{O}_2$  mixed gases (4:1) using a WaferMasters SRTF-201LP system. The samples ( $\sim 3\text{cm} \times 3\text{cm}$ ) for Raman scattering measurement were cut from the 200 mm wafers.

The samples were analyzed by Raman scattering measurements at room temperature. The UV and visible lasers at 266.0 nm, 363.8 nm, and 457.9 nm were used as an excitation source to analyze the crystallinity in the depth direction in the implanted-samples. The laser penetration depths into the Si wafer ( $=1/a$ , with  $a$  being the optical absorption coefficient) are estimated as 5, 10 and 300 nm, respectively, and have the following meaning: when back-scattered photons are observed, about 90% of the signal emanates from the region between the surface and the penetration depth.

## Results and discussions

Figure 1 (a) and (b) show Raman spectra for Si wafers implanted with  $^{11}\text{B}$  of  $2 \times 10^{14}$  and  $2 \times 10^{15} \text{ cm}^{-2}$  using different excitation wavelengths as the excitation source. The inserts show the peak frequency and the full width at half maximum (FWHM) of a Si phonon signal for B-implanted Si wafer samples. In both samples shown in Fig. 1 (a) and (b), Si phonon signals at  $520 \text{ cm}^{-1}$  were shifted to lower frequency and its FWHM increased with decrease in excitation wavelength. As mentioned, the probe depth can be varied by using different wavelength for excitation. The laser penetration depth in Si is roughly estimated at 5, 10, 300 nm using laser wavelength at 266.0, 363.8, 457.9 nm, respectively. The Raman spectrum gives information as to the crystallinity of the surface region using the UV laser. While the Raman signals from the shallower penetration depths (using 266.0 and 363.8 nm) have significant contribution from the surface region, the Raman signal from 457.9 nm irradiation (visible region) is dominated by the contribution from deeper regions of the silicon and gives crystallinity insight from interior wafer regions.

From these reasons, the peak shift to the lower frequency side and the increase of FWHM indicate the deterioration of the crystallinity of the Si host lattice caused by B ion implantation. These features become prominent with increases in B implantation level as shown in Fig. 1 (b). On the other hand, in the Raman spectrum using excitation wavelength at 266.0 nm, shown in Fig. 1(b), the peak has asymmetric shape tailed to the lower frequency side. An additional broad signal was also observed at  $\sim 490 \text{ cm}^{-1}$ , shown as the dotted line in Fig. 1 (b). These features were also observed in Fig. 1 (a). These results indicate that the crystallinity of the surface region was seriously deteriorated and the amorphous Si was formed from B ion implantation at the surface.

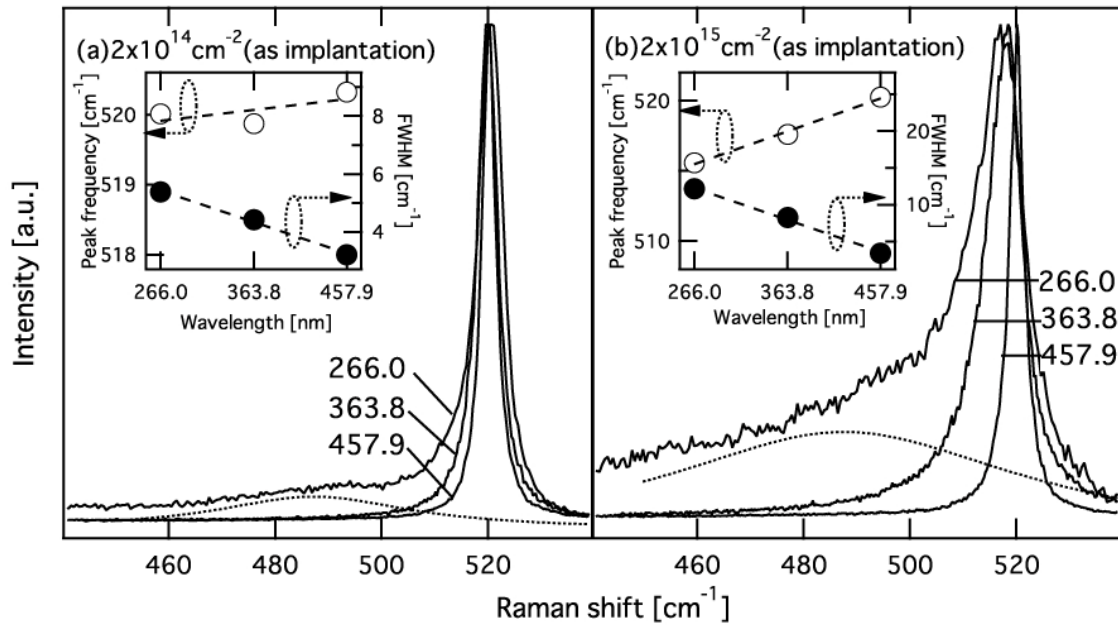


Figure 1. Raman spectra for samples implanted with B of  $2 \times 10^{14} \text{ cm}^{-2}$  (a) and  $2 \times 10^{15} \text{ cm}^{-2}$  (b) using different wavelengths for excitation source. The peak frequency and the FWHM of Raman signal are plotted in the inserts. The dotted line is the signal of amorphous Si.

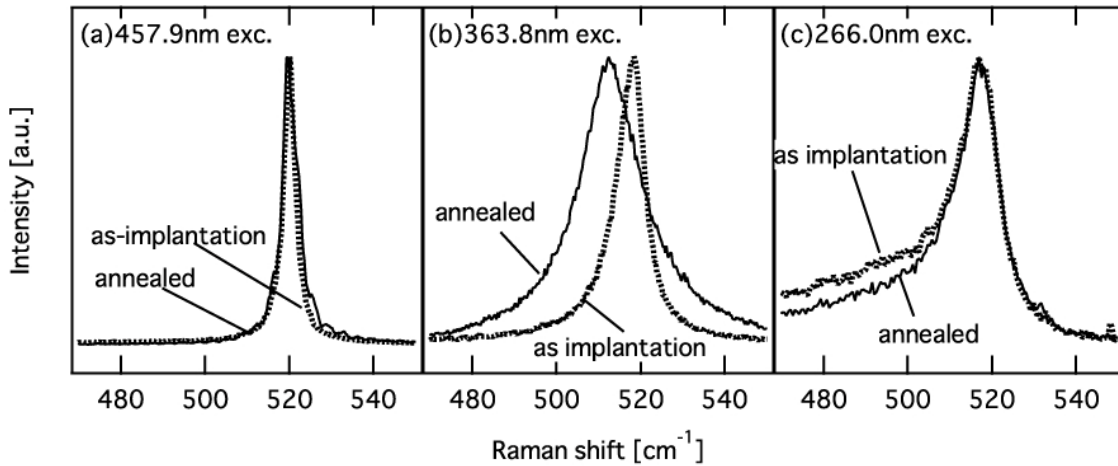


Figure 2. Raman spectra for the samples implanted with B of  $2 \times 10^{15} \text{ cm}^{-2}$  and annealed at 1025°C for 10 sec in N<sub>2</sub> atmosphere using different excitation wavelengths at 457.9 nm (a), 363.8 nm (b) and 266.0 nm (c).

Figure 2 (a), (b) and (c) show Raman spectra for the samples implanted with B of  $2 \times 10^{15} \text{ cm}^{-2}$  and annealed at 1025°C for 10 sec in an N<sub>2</sub> atmosphere using different excitation wavelengths. For comparison, Fig. 2 (a), (b) and (c) include Raman spectra for as-implanted samples. Significant change was not observed in Fig. 2 (a), because the signals are dominated by the deeper regions of the Si wafers by using the visible laser at 457.9 nm. On the other side, in Fig. 2 (c), the broad signal related to the amorphous Si decreases in intensity by the thermal annealing, suggesting that the crystallinity of the surface region was improved by the recrystallization of amorphous Si. Furthermore, Raman spectra were drastically changed by excitation at 364.8 nm as shown in Fig. 2 (b).

The peak was considerably shifted to the lower frequency side and drastically broadened. But retaining symmetry, showing that the Si host lattice loses the lattice periodicity and remains under tensile stress. Figure 3 shows the local vibrational mode related to B using 363.8 nm excitation, showing increased intensity following thermal annealing. This indicates that B density at 10 nm depth increased by the thermal annealing. These results show that implanted B, which peaks at a depth of 20 nm, was defused from 20 nm in depth to 10 nm by the thermal annealing.

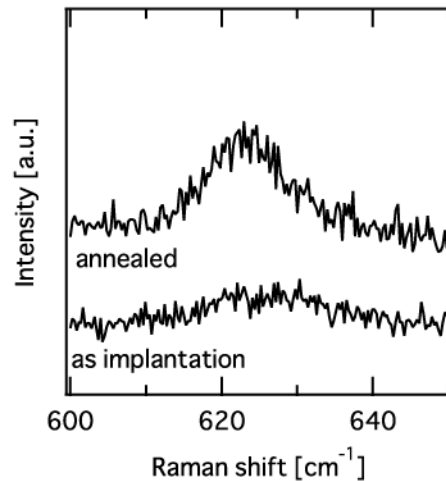


Figure 3. Local vibrational modes related to B for the samples implanted with B of  $2 \times 10^{15} \text{ cm}^{-2}$  and annealed at  $1025^\circ\text{C}$  for 10 sec in  $\text{N}_2$  atmosphere.

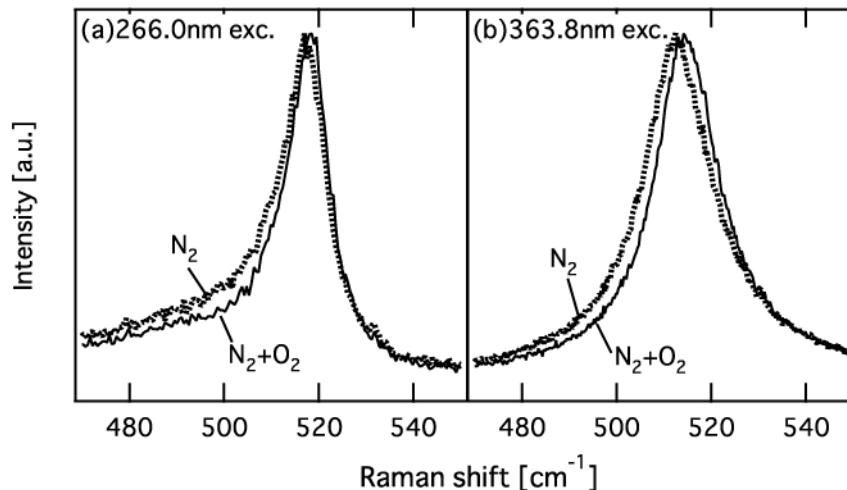


Figure 4. Raman spectra for the samples annealed at  $1025^\circ\text{C}$  for 10 seconds in  $\text{N}_2$  or  $\text{N}_2$  and  $\text{O}_2$  mixed gas atmosphere using different excitation wavelength at 266.0 nm (a) and 363.8 nm (b).

Then, the samples were annealed at  $1025^\circ\text{C}$  for 10 sec in  $\text{N}_2$  and  $\text{O}_2$  mixed gas atmosphere. Raman spectra using 266.0 nm and 363.8 nm for an excitation are shown in Figs. 4 (a) and (b), respectively. For comparison, Figs. 4 (a) and (b) include the Raman spectrum for the samples annealed in  $\text{N}_2$  atmosphere. In Fig. 4 (a), the peak was slightly shifted to the higher frequency side and the FWHM of Raman signal decreased by the thermal annealing in an  $\text{N}_2$  and  $\text{O}_2$  mixed gas atmosphere. Furthermore, as shown in Fig. 4 (b), simi-

lar behaviors were also observed using 363.8 nm for excitation, showing that B density at a depth of 10 nm decreased compared with the sample annealed in an N<sub>2</sub> atmosphere. The broad signal related to the amorphous Si decreased in intensity as shown in Fig. 4 (a). These results indicate that the recrystallization of surface amorphous Si promoted while the diffusion of implanted B was suppressed using N<sub>2</sub> and O<sub>2</sub> mixed gas as an annealing atmosphere.

Finally, the samples implanted with B of  $2 \times 10^{15} \text{ cm}^{-2}$  were annealed at various temperatures for 40 sec in N<sub>2</sub> and O<sub>2</sub> mixed gas atmosphere. The annealing temperature was varied in the range of 1005°C to 1045°C. Figure 5 (a) and (b) show the peak frequency and the FWHM of Raman signals using 363.8 nm and 457.9 nm for an excitation, respectively. In both cases, it was observed that the peak shifts to the lower frequency side and the FWHM of the Raman signal broadens with increase in annealing temperature, indicating that implanted B was more diffused in both directions from the implanted depth with increase in annealing temperature. Furthermore, Fig. 6 (a) shows the peak frequency and the FWHM of Raman signals using 266.0 nm for excitation. With increase in annealing temperature up to 1025°C, the peak shifted slightly to the lower frequency side and the FWHM increased monotonically. As shown in Fig. 4 (a), however, the peak shifts to the higher frequency side and the FWHM of Raman signal decreased by thermal annealing due to the recrystallization of amorphous Si at the surface. One might expect to enhance these features with increase in annealing temperature, but, the result shown in Fig. 6(a) indicates the opposite results. This contradictory finding may be caused by different annealing time. With increase in annealing time, although the diffusion of B was suppressed more using N<sub>2</sub> and O<sub>2</sub> mixed gas, implanted B diffused to the surface by thermal annealing for 40 sec. In fact, the peak shift and the broadening shown in Fig. 6(a) may be caused by this. These behaviors were also observed for the sample annealed in N<sub>2</sub> atmosphere as shown in Fig. 6(b). On the other hand, for the samples annealed above 1025°C, it was observed that the peak shifts to the higher frequency side and the FWHM of Raman signal decreased with increase in annealing temperature in Fig. 6(a) and (b). Here, recalling that implanted B was diffused enough to the surface with annealing below 1025 °C, these features suggest the decrease in B density at the surface. In fact, a thin layer with low B density is formed at the top surface by the evaporation of B from the Si wafer.

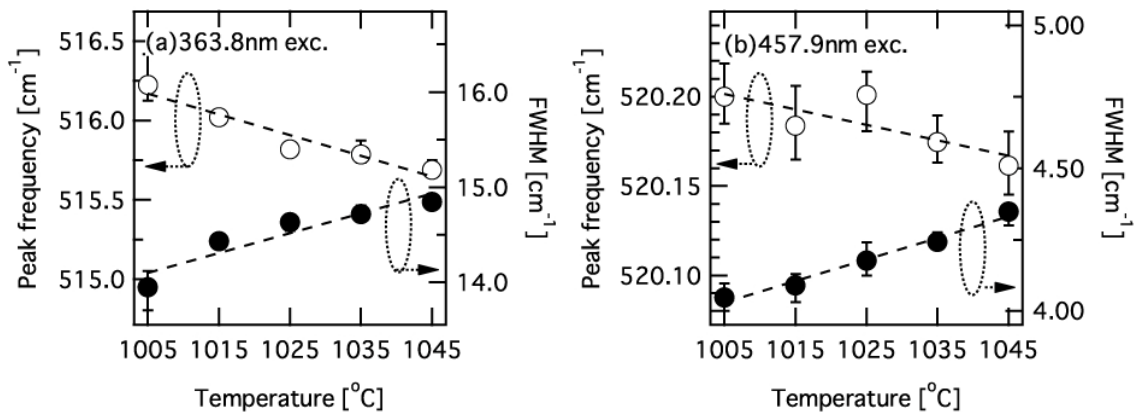


Figure 5. The dependence of the peak frequency and the FWHM of Raman signal on annealing temperature using different excitation wavelength at 363.8 nm (a) and 457.9 nm (b). The samples were annealed for 40 sec in N<sub>2</sub> and O<sub>2</sub> mixed gas atmosphere.

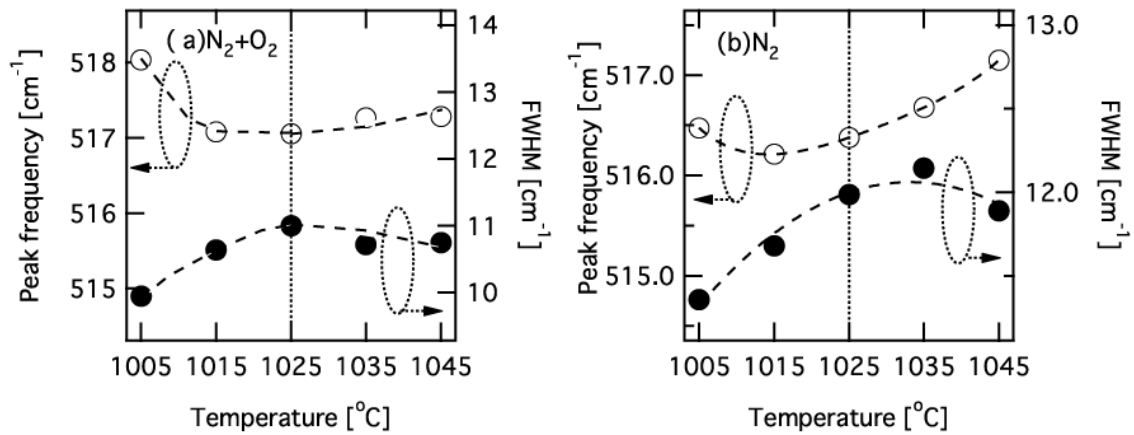


Figure 6. The dependence of the peak frequency and the FWHM of Raman signal on annealing temperature using 266.0 nm for excitation. The samples were annealed for 40 sec in N<sub>2</sub> and O<sub>2</sub> mixed gas (a) or N<sub>2</sub> gas (b) as an annealing atmosphere.

### Summary

Ultra-shallow B-implanted Si wafers were investigated by Raman scattering using UV and visible lasers for excitation. Variation of crystallinity and impurity diffusion with depth were analyzed by selecting the wavelength of the excitation laser, and the annealing effects were also investigated by changing the annealing temperature, time and environment.

The crystallinity of the samples deteriorated with increase in B implantation level. The crystallinity of the top surface region was seriously deteriorated and amorphous Si was observed at the top surface region. By the thermal annealing, the surface amorphous Si was recrystallized, and the implanted B, with density peaks at the depth of 20 nm was diffused to the depth of 10 nm from the surface. Furthermore, it was observed that the recrystallization of surface amorphous Si was promoted and the diffusion of implanted B was suppressed using N<sub>2</sub> and O<sub>2</sub> mixed gas as an anneal atmosphere. Finally, it was confirmed that the implanted B was diffused enough to the top surface with increase in annealing temperature. However, a thin layer with low B density was observed at the surface for the samples annealed above 1025°C, suggesting the evaporation of B from the Si wafer at the surface region.

### Acknowledgement

The authors would like to thank Mr. Y. Baba of Panasonic Semiconductor Eng. Co. Ltd, Ms. E. Kanazaki, Mr. F. Kawase and Mr. S. Shibata of Panasonic Corp. Semiconductor Co. Ltd. for providing valuable specimens and useful discussions throughout this work. The authors would also like to thank Mr. S. Takashima of Kyoto Institute of Technology for useful technical discussions.

## References

- [1] M. Yoshimoto, H. Nishigaki, H. Harima, T. Isshiki, K. Kang and W.S. Yoo, *J. Electrochem. Soc.* 153 G679 (2006)
- [2] T. Gebel, M. Voelskow, W. Skorupa, G. Mannino, V. Privitera, F. Priolo, E. Napolitani, and A. Carnera, *Nucl. Instrum. Methods Phys. Res. B* 186, 287 (2002).
- [3] K. Shibahara, H. Furumoto, K. Egusa, M. Koh and S. Yokoyama, *Mater. Res. Soc. Symp. Proc.* vol. 532, pp. 23-28 (1998)
- [4] H. Richter, Z. P. Wang, and L. Ley, *Solid State Commun.* 39, 625 (1981)
- [5] F. Cerdeira, C. J. Buchenauer, F. H. Pollak and M. Cardona, *Phys. Rev. B* 5, 580 (1972)
- [6] J. F. Ziegler, J. P. Biersack, and U. Littmark, *The Stopping and Range of Ions in Solids*, Pergamon Press, New York (1985), and <http://www.srim.org/>